Chapter 8

Types of cavitation: ARTIFICIAL ROUGHNESS AND INCEPTION OF SHEET CAVITATION

Objective: *Description of the application of leading edge roughness and its effects*

The ultimate goal of cavitation investigations at model scale is the prediction of full scale cavitation behavior. That means prediction of cavitation behavior at high Reynolds numbers with ample nuclei. The problems with lack of nuclei and with laminar boundary layers are complications raised by model testing. There are two ways to deal with these complications. The first way is to control the complications and to "correct" model scale results for the differences between model and full scale, such as the correction of the viscous model drag to extrapolate ship resistance to full scale. The second way is to develop model scale techniques to avoid these complications. For cavitation inception this would mean supply of ample nuclei of the proper size and avoidance of laminar boundary layer flow.

8.1 Paint Tests

Avoidance of laminar flow has been the basis of the ITTC recommendation to use a minimum Reynolds number of $2 * 10^5$ on propeller sections. In many cases, depending on the pressure distribution, this minimum Reynolds number does not avoid laminar flow. In uniform flow this can be checked by a "paint test", in which a thick layer of "paint" is applied at the leading edge of a propeller model (Fig. 8.1)

The "paint" is not real paint in that it is supposed not to dry rapidly. The propeller is then mounted in a tunnel or a towing tank and run in a certain condition for a short time. The time should be enough for the paint to be spread out by the flow over the blade, as in Fig 8.2. In this picture the paint was mixed with fluorescent dye, so that the very thin paint layer was better visualized when illuminated with ultra-violet light.

The pattern in this figures is caused by two forces on the paint particles. The first force is the friction force between the paint and the water, which is directed in chordwize direction. The paint is moving very slowly relative to the propeller, and is therefore subject to a centrifugal force , which is directed in outward radial direction. The result is that the paint will move outward. In a region with laminar boundary layer flow the friction force is smaller than in a region with turbulent boundary layer. This results in a change in direction of the paint streaks: in

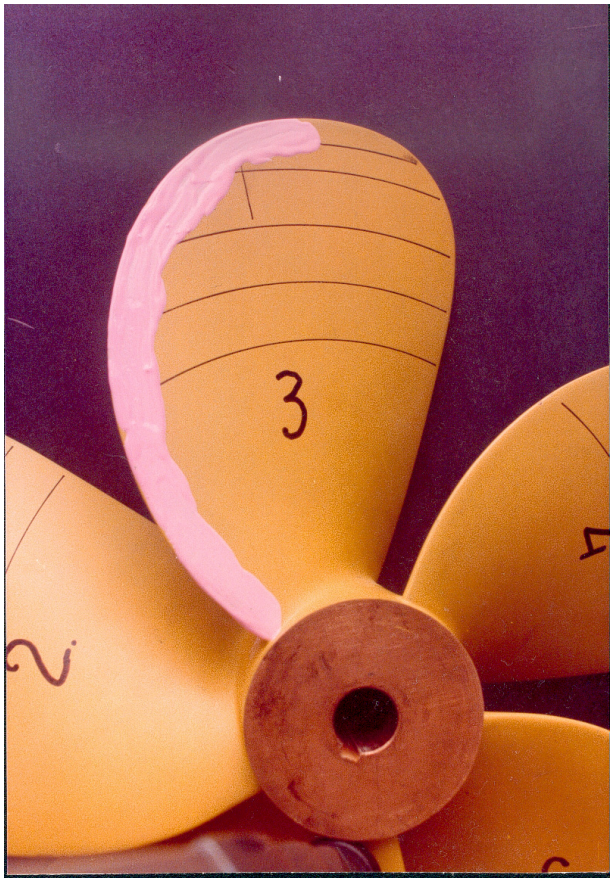

Figure 8.1: Application of paint

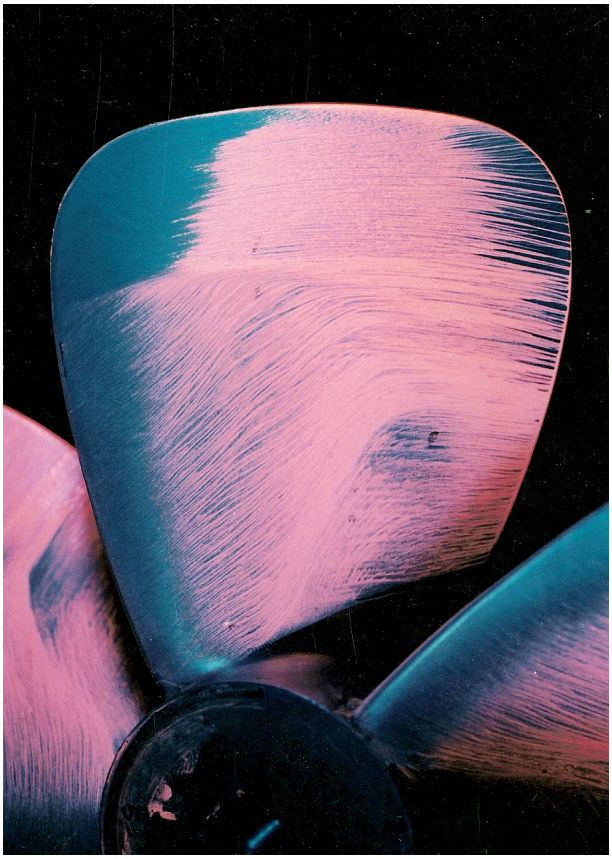

Figure 8.2: Paint test on propeller of Fig. 7.4

regions with a turbulent boundary layer the paint streaks will be close to the tangential direction. In regions with laminar boundary layer flow the streaks will be pointed outward. And in regions with separated flow there will be no paint at all or the paint streaks will be directed radially outwards. This makes it possible to distinguish various boundary layer regimes on a propeller blade.

The pattern shows an abrupt change in the direction of the paint streaks at a certain radius. Outside that radius the paint streaks are in chordwise direction, which indicates a turbulent boundary layer flow from the leading edge on. This is caused by a laminar separation bubble at the leading edge. A laminar separation bubble occurs when the boundary layer separates near the leading edge due to a strong low pressure peak there. At separation the boundary layer is still laminar. However, the separated laminar boundary layer is unstable and becomes turbulent soon after separation. The turbulent boundary layer causes the turbulent boundary layer to reattach to the surface and the boundary layer is thus turbulent from there on. A sketch of a short laminar separation bubble is given in Fig. 8.3.

Paint tests revealed that for most propellers the criterion as used by the

When the pressure peak becomes strong and the adverse pressure gradient downstream of the minimum pressure becomes very adverse the separation bubble can become long and reattachment takes place in the midchord region of the section. If no reattachment takes place the profile is *stalled*.
In some cases the laminar separation bubble

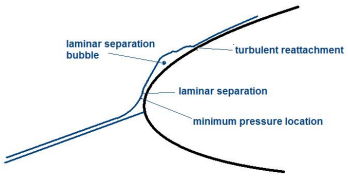

Figure 8.3: A short laminar separation bubble

is revealed by the paint test by a thin line of paint at the leading edge. Mostly the laminar separation bubble is too short to be visible.

Laminar separation is independent of the Reynolds number. A confirmation of the fact that laminar separation is involved is that the radius at which the paint lines suddenly become tangential is independent of variations in the Reynolds number. On the other hand this radius is very sensitive to variations in propeller loading. This radius could be predicted by two-dimensional boundary layer calculations on propeller blade sections ([33]). So the role of laminar separation has been confirmed in various ways.

Fig 8.2 shows that inside of the radius of laminar separation there is a significant area of laminar flow. Transition to turbulence is indicated by a rather corner where the outward directed paint streaks change into tangential lines. In Fig. 8.2 the boundary layer in the low pressure region near the leading edge at inner radii is fully laminar. At the root the flow is close to separation. The friction force becomes very low there, resulting in a collection of paint in that region. The direction of the paint streaks is not yet fully radial, indicating that no separation

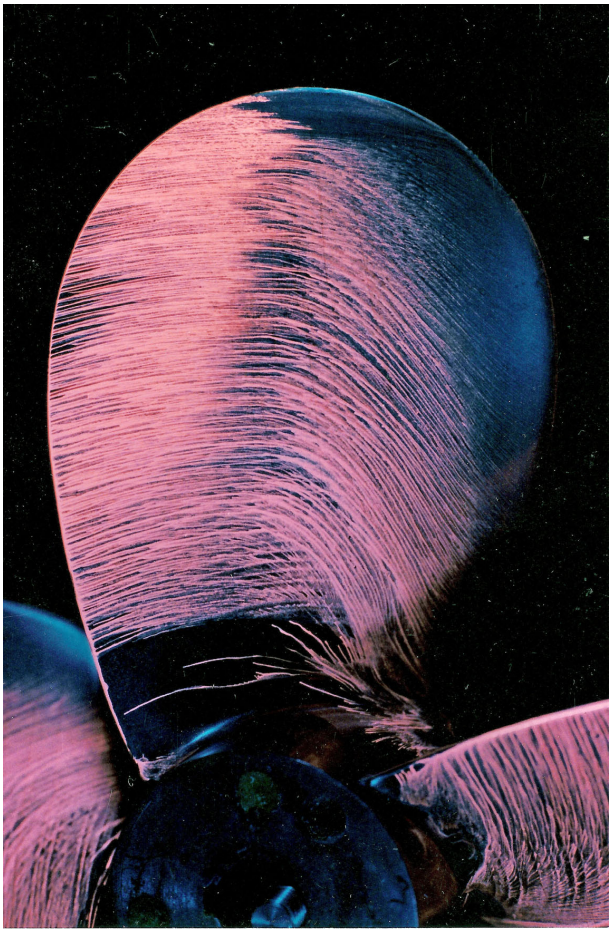

Figure 8.4: Paint pattern on the pressure side of a conventional propeller

occured yet. This is confirmed by the fact that there are paint streaks downstream of that region with thick paint.

The transition is not always as sharp as in the previous pictures. Especially at the pressure side the direction of the paint streaks changes more gradually. So the transition region is much longer in that case (Fig 8.4).

An increase of the Reynolds number in propeller testing is not very effective. The location of transition depends more on the pressure distribution than on the Reynolds number. When the local pressure gradient is favorable, it is very difficult to generate transition. A paint test at a very high Reynolds

number is shown in Fig shown in Fig. 7.5. The result is not that the transition location has moved much towards the leading edge. However, turbulent streaks occur instead in the region of the laminar boundary layer. This is due to the fact that the high Reynolds number makes the boundary layer thinner and thus more susceptible to surface irregularities. The turbulent streaks originate at irregular spots on the surface of the propeller. This can also be simulated with larger irregularities on the surface and application of leading edge roughness is therefore a logical simulation of a high Reynolds number.

8.2 Turbulence Stimulators

Artificial stimulation of turbulence is a well known way of creating a turbulent boundary layer. It is applied in airplanes to prevent separation, generally by small triangles at an angle with the flow. A turbulent boundary layer is also stimulated at the bow of ship models, where trip wires or studs (cylinders vertical to the surface) are used. To understand the effect of turbulence stimulators the mechanism of transition has to be understood in more detail, although it should be kept in mind that this description is very simplified and many details are still unknown.

Transition to turbulence occurs in the laminar boundary layer after at some point the boundary layer becomes unstable. This instability means that small disturbances in the velocity (e.g. due to turbulence) are magnified. After some distance the magnification is so large that the boundary layer becomes turbulent. The region between the location where the boundary layer becomes unstable and the location of fully developed turbulence is the transition region. In the transition region only a specific bandwidth of disturbances is amplified. Al disturbances outside this bandwidth are damped out and will disappear. As a result the transition region contains waves of velocity fluctuations, the so called "Tollmien-Schlichting" waves. The magnification of disturbances in a laminar boundary layer is very local, leading to so-called turbulent bursts in the boundary layer.

At a small distance downstream of a single roughness element the shape of the velocities in the boundary layer is similar to the boundary layer without roughness. But the fluctuations of the velocity are increased. So the mechanism of turbulence stimulation seems to be through the enhanced instability [25].

The effects of roughness on flat foils has been studied extensively, but mostly with the focus on maximum lift or stall. However, in case of cavitation inception there is an important additional requirement: the local mean pressure should not be affected. It means the stimulator should be small. Investigations of a trip wire [15], [2] were not very satisfactory, because the trip wire was causing a separated region which was Reynolds dependent and dependent on the size of the trip wire. So the inception conditions were too dependent on the location and the size of the trip wire. It was already found by Klebanov et al [25] that three dimensional roughness was less dependent on the Reynolds number and caused transition depending on the roughness Reynolds number

$$Re_\theta = \frac{v_k k}{\nu} \tag{8.1}$$

where v_k is the velocity at the top of the roughness in the absence of roughness and k is the height of the roughness. The value of the roughness Reynolds number causing transition to turbulence was between 500 and 750. These numbers were obtained on a flat plate, so without pressure gradient.

Distributed carborundum particles proved

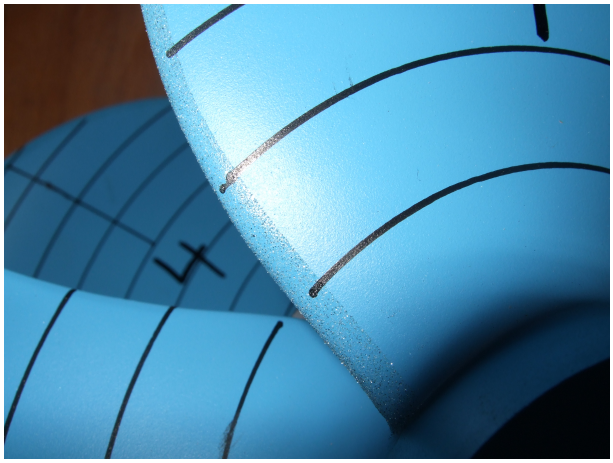

Figure 8.5: Leading edge roughness on a propeller model

to be more successful in cavitation inception tests in the Depressurized Towing Tank [33], [34] and this technique will be discussed in more detail. In case of leading edge roughness turbulence stimulation is done by distributed roughness particles which are glued to the surface over a certain length near the leading edge of a foil.

8.3 Application of leading edge roughness

The first requirement in the application of turbulence stimulator is that the mean pressure over the blade section is not affected. This is a relative statement, because the difference in Reynolds number between model and full scale also causes differences in the mean pressure, as does the occurrence of a laminar separation bubble. In fact a laminar separation bubble can also be considered as a turbulence stimulator.
It means that the size of the roughness has to be small. There is insufficient knowledge about the precise mechanism of roughness elements in a boundary layer, but an experimentally determined criterion is that the roughness Reynolds number should exceed 120 to be effective [10]. The roughness Reynolds number is defined as

$$\frac{V * k}{\nu} \tag{8.2}$$

in which V is the fluid velocity outside the boundary layer at the location of the roughness and k is the height of the roughness elements. At a typical velocity of 10 m/sec this leads to a minimum roughness height of 12 microns. For roughness to be effective Ligtelijn [37]found a minimum roughness Reynolds number of 300. In practice the size of the roughness elements used in a cavitation tunnel (with a high Reynold number) the roughness size can be taken as 30 microns. In a Depressurized Towing Tank the roughness size is taken 60 microns.

The carborundum size and the roughness height are not necessarily the same. Roughness particles have to be attached to the foil surface and this is generally done by some glue. It is important that the glue is not smoothing the area between the roughness elements. The best way to avoid that is to take watery thin glue and to keep the roughness particles at some distance of each other. As a rule of thumb the coverage of the roughness elements should not exceed 50 percent of the area. An example of leading edge roughness properly applied is given in Fig. 8.6.

Application of small roughness elements is often difficult, because the particles tend to clog together. A way to apply distributed roughness elements is to blow air with particles over an area with freshly applied glue. To avoid a disturbance in the mean pressure the glue should be very thin.

As roughness elements carborundum particles are often used. These particles, also used

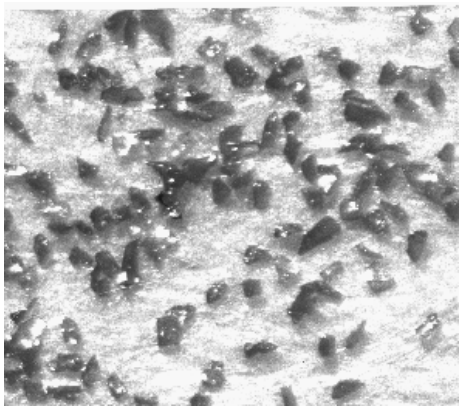

Figure 8.6: Distribution of roughness particles in leading edge roughness

in grinding paper, have sharp contours, which make them effective for cavitation inception. An alternative is spherical balls, but these are less effective in generating cavitation inception. Other turbulence stimulators like zigzag paper have the same drawback as a trip wire: a rather sharp beginning and end, causing local separation and a disturbance in the mean pressure.

The length of application of leading edge roughness depends on the pressure distribution. In general it can be stated that it is very difficult to cause transition in a strongly favorable pressure gradient, as occurs upstream of a minimum pressure location. So the extent of the roughness should cover the minimum pressure location, in order to generate transition shortly downstream of this location. On ship propeller models the location of the minimum pressure is very close to the leading edge. In that case coverage of the leading edge roughness over some 2% of the chord is enough. A further extension of the coverage is undesirable because of the increasing effect of the roughness on sectional drag, but at inner radii the leading edge is thicker and the minimum pressure further away from the leading edge. There the extent of the roughness has to be larger.

8.4 Cavitation inception on roughness elements

Cavitation inception on roughness elements in a low pressure peak occurs typically by small spots of cavitation, as shown in Fig. 8.7 (A foil at 5 degrees angle of attack).In this figure the angle of attack is not high and the pressure at the leading edge is low over the whole roughened region. The small spots are evidently caused by the roughness elements. Their size exceeds already the size of the roughness elements, however, which means that the mean pressure outside the boundary layer is close to the vapor pressure. When the angle of attack is higher and the low pressure peak is close to the leading edge, the roughened region is longer than the low pressure peak. This will result in the inception of cavitation spots at the leading edge, as shown in Fig. 8.8(the same foil at 8 degrees angle of attack). When the pressure in Fig. 8.8 was increased gradually the spots would become smaller, but long before the length approached zero they would suddenly disappear. From that we may conclude that local separation at a roughness element induces inception. The inception condition will be when the reattachment pressure reaches the vapor pressure. The mean pressure at the inception location outside the boundary layer will then also be close to the vapor pressure, when the carborundum grains are evenly distributed. It explains why sharp carborundum particles are more suitable for stimulation of cavitation inception, because the flow separates more readily.

The problem remains when to call inception. Looking very closely to the first minute cavitation spots on the roughness elements makes that the inception pressure depends too much on the local roughness element. Such spots may occur locally up to high pressures. However, in such cases the spots are not very sensitive to pressure variations. They persist up to higher pressures. When the pressure is lowered

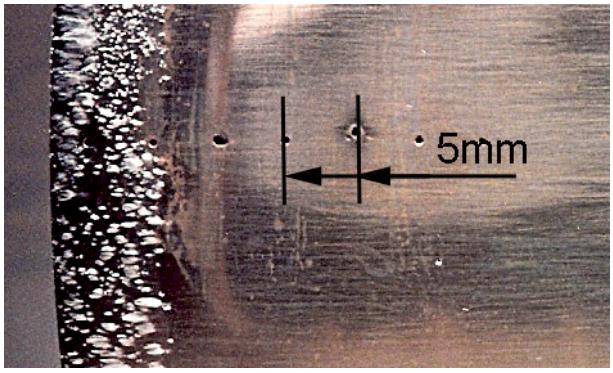

Figure 8.7: Cavitation inception on roughness elements

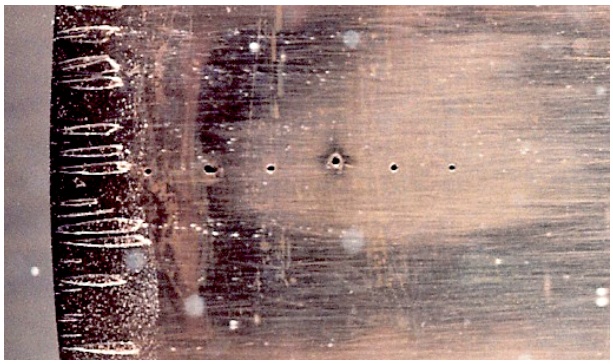

Figure 8.8: Cavitation inception on roughness elements

the inception pressure is therefore called when the spots begin to grow significantly with decreasing pressure. Fig. 8.8 is a situation which is close to the inception pressure. This picture illustrates that it is not useful to detect cavitation inception on the first tiny spot which occurs, because this will probably depend only on the size of the local roughness element.
It will be clear that acoustic inception on roughness elements can be considerable earlier than visual inception.

8.5 Effects of leading edge roughness on propeller performance

The main effect on propulsion of a laminar boundary layer on propeller sections will be a reduction of the sectional drag. This will reduce both torque and thrust, but especially the thrust. The effect will be a slight increase of the efficiency of the propeller. When leading edge roughness is applied two effects are introduced: -restoration of the turbulent boundary layer, resulting in a restoration of the turbulent drag of the blad sections -additional drag of the roughness elements. The last effect cannot be distinguished from the first effect. However, since the area of roughness is only very small the effect is expected to be small.

This turns out to be a simplification of the real flow around blade sections at model scale. Measurements of propeller thrust and torque often show that the torque increases with roughness and the efficiency drops with a few percent. However,the viscous effects on torque and thrust of a propeller model may be more complicated. Sometimes the sectional thrust is affected by the laminar flow, leading to a change in thrust. This may be in both directions, and the relation with the pressure distribution is not yet fully clear.

Sometimes the thrust increases with the application of roughness. This is especially the case when the blade loading is at the trailing edge, so when there is a strong pressure gradient at the suction side near the trailing edge. In such a case the flow an the smooth blade separates earlier than on the roughened blade, resulting in an increase in sectional lift coefficient when the boundary layer is turbulent. Then the efficiency increases slightly with the application of roughness. For the extrapolation to full scale is can be expected that the roughened performance is representative for full scale, eventually after some correction for Reynolds number effects has been applied to

the sectional drag (see ITTC 1978, [21]).

Bibliography

[1] Arakeri,V.H., Acosta, A.J., 1979, *Viscous Effects in the Inception of Cavitation*, A.S.M.E. Int. Symposium on Cavitation, New York, USA.

[2] Arndt, R.E.A., 1976, *Cavitation on Model Propellers with Boundary Layer Trips*, A.S.M.E.Conference on Polyphase Flow, New Orleans, USA.

[3] Arndt, R.E.A., Ellis, C.R., Paul, S. 1995, *Preliminary Investigation of the Use of Air Injection to mitigate Cavitation Erosion*, A.S.M.E. Journal of Fluids Engineering, Vol.117.

[4] Briggs, L.J., 1950 *Limiting negative pressure of water.*, J. Applied Phys. 21:721722.

[5] Brennen, C.E., 1995 *Cavitation and Bubble Dynamics*, Oxford University Press, ISBN 0-19-509409-3. Also available on internet.

[6] Burrill, L.C., 1951, *Sir Charles Parsons and Cavitation*, Transactions of the Institute of Marine Engineers.

[7] Borkent, B.M., 2009, *Interfacial Phenomena in Micro- and Nanofluidics: nanobubbles,cavitation, and wetting*, Thisis Twente University, The Netherlands.

[8] Coutier-Delgosha, O., Devillers, J-P., Leriche, M., Pichon, T., 2005, emphEffect of Roughness on the Dynamics of Unsteady Cavitation, Journal of Fluids Eng. , vol 127.

[9] Epstein, P.S., Plesset, M.S. 1950 *On the stability of Gas Bubbles in Liquis-Gas Solutions*, Journal of Chemical Physics, Vol.18., pp1505-1509.

[10] , Feindt, E.G., 1956,*Untersuchungen uber die Abhangigkeit des Umschlages Laminar-Turbulent von der Oberflachenrauhigkeit und der Druckverteilung*, Jahrbuch STG, Bd.50, pp180-205

[11] Flynn, H.G., 1964, *Physics of Acoustic Cavitation*, W.P.Mason ed. Vol1,PartB,Academic Press New York-London.

[12] Foeth, E-J., Kuiper, G. 2004, *Exploratory experiments to determine flow and structure borne noise of erosive cavity implosions*, A¿S¿M¿E¿ Fluids Eng. Summer Conference, HT-FED2004-56789, Charlotte, NC. USA.

[13] Foeth, E-J., *The Structure of Three-Dimensional Sheet Cavitation*, Thesis Technical University Delft.

[14] Fox, F.E., Herzfeld, K.F., 1954 *Gas Bubbles with Organic Skin as Cavitation Nuclei*, J.Acoust. Soc. Am. Vol.26, pp 984-989.

[15] Gates, E.M., 1977 *(* The influence of Free-Stream Turbulence, Free Stream Nuclei Populations and a Drag-reducing Polymer on Cavitation Inception on Two Axisymmetric Bodies California Institute of Technology, Rep. No. Eng 183-2.

[16] Harvey, E.N., McElroy, W.D., Whiteley, A.H., 1947 *On Cavity Formation in Water*, Journal of Applied Physics, Vol.18, pp162-172.

[17] Hoekstra, M., Vaz, G. *The Paartial Cavity on a @D Foil Revisited*, 7th Int. Conference on Cavitation CAV2009, Ann Arbor, Michigan, U.S.A.

[18] Holl, J.W., 1960, *An Effect of Air Content on the Occurrence of Cavitation*, Trans. A.S.M.E., Journal of Basic Eng. Vol.82, pp941-946.

[19] Holl, J.W., Carrol, J.A., 1981, *Observations of the Various Types of Limited Cavitation on Axisymmetric Bodies*, PUB A.S.M.E. Journal of Fluids Eng.,Vol 103,pp415-423

[20] Huang, T.T., 1981, *Cavitation Inception Observations on Six Axisymmetric Headforms*, A.S.M.E. Journal of Fluids Engineering, Vol 103,PP273-278

[21] ITTC, 1978,Proceedings 15th ITTC, The Haque, Report of the Performance Committee.

[22] Johnsson, C.A., Hsieh,T., 1966, *The Influence of Trajectories of Gas Nuclei on Cavitation Inception*, 6th Symposium on Naval Hydrodynamics, Washington D.C., pp163-178.

[23] Takagi,K., Kato,H.,Kato,D.,Sugimoto, A., 2006, *Destruction of Plankton by Two-Dimensional Cavitating Jet*, Sixth International Symposium on Cavitation CAV2006, Wageningen, The Netherlands.

[24] Keller, A.P., 1974 *Investigations Concerning Scale Effects of the Inception of Cavitation*, Proc. I.Mech.Eng. Conference on Cavitation, Edinburgh, 109-117.

[25] KLEBANOFF, P.S., SCHUBAUER, G.B., TIDSTROM,K.D., 1955, *Measurements of the Effect of Two-dimensional and Three-dimensional Roughness Elements on Boundary Layer Transition*, J. Aeron. Sciences

[26] Knapp, R.T., Hollander, A., 1948, *Laboratory Investigations of the Mechanism of Cavitation*, Trans. A.S.M.E., Vol.70, pp.419-435.

[27] Knapp, R.T., Daily, J.W., Hammitt, F.G., 1970, *C*avitation, New York : McGraw-Hill.

[28] Knapp, R.T., Hollander, A., 1948, *L*aboratory Investigations of the Mechanism of Cavitation, Trans. A.S.M.E., Vol 70, pp419-435.

[29] Korkut, E., Atlar, M., 2000, *On the Importance of Effect of Turbulence in Cavitation Inception Tests of Marine Propellers*, Proceedings of Royal Society of London A: Mathematical, Physical and Engineering Sciences, Vol.458 , pp.29-48.

[30] Kreider, W., Crum, L., Bailey,M., Matula, T.,Khoklova, V., Sapozhnikov,O., 2006, *Acoustic Cavitation and Medical Ultrasound*,Sixth International Symposium on Cavitation CAV2006, Wageningen, The Netherlands.

[31] Kumar, S., Brennen, C.E., 1996, *A Study of Pressure Pulses generated by Travelling Bubble Cavitation*, Journal of Fluid Mechanics Vol 255 pp541.

[32] Hwansung Lee, Tomonori Tsukiya, Akihiko Homma, Tadayuki Kamimura,Eisuke Tatsumi, Yoshiyuki Taenaka, Hisateru Takano, *Observation of Cavitation in a Mechanical Heart Valve*, Fifth International Symposium on Cavitation (cav2003),Osaka, Japan.

[33] Kuiper, G., 1978, *Scale Effects on Propeller Cavitation*, 12th Symposium on Naval Hydrodynamics, Washington D.C., USA.

[34] Kuiper, G. 1981, *Cavitation Inception on Ship Propeller Models*, Thesis Technical University Delft.

[35] Kuiper, G. 2008, *Fundamentals of Ship Resistance and Propulsion*, Course Lectures Technical University Delft.

[36] Landa, E.R., Nimmo, J.R.,2003 *The Life and Scientific Contributions of Lyman J. Briggs*, Journal of the Soil Science Society of America, Vol 67 no 3, pp 681-693. http://soil.scijournals.org/cgi/reprint/67/3/681

[37] Ligtelijn, J.T., van der Kooij, J., Kuiper, G., van Gent,W., 1992, *Research on Propeller-Hull Interaction in the Depressurized Towing Tank*, Hydrodynamics, Computations,Model Tests and Reality (Marin), Elseviers Science Publishers.

[38] Morch E.M., 2000, Paper on Cav2003.

[39] Moerch, K.A. 2009, *C*avitation Nuclei: Experiment and Theory,Journal of Hydrodynamics Vol21 p176.

[40] Neppiras, E.A., Noltink, B.E., 1951, *Cavitation produced by Ultrasonics*, Proc. Phys. Soc. London, pp 1032-1038.

[41] Ohl, C-D., Arora, M. ,Roy, I., Delius. M., Wolfrum, B.,2003, *Drug Delivery Following Shock Wave Induced Cavitation* , Fifth International Symposium on Cavitation (cav2003),Osaka, Japan.

[42] Plesset, M.S., 1949, *The Dynamics of Cavitation Bubbles*, ASME Journal of Appl. Mech. 1949, pp 277-232.

[43] Schiebe, F.R., 1972, *Measurement of the Cavitation Susceptibility of Water using Standard Bodies*, St. Anthony Fall Hydraulic Lab, Univ. of Minnesota, report 118.

[44] Schlichting, H., 1968, *Boundary Layer Theory*, McGraw-Hill, 6th edition.

[45] Terwisga, T.J.C., Fitzsimmons, P.A., Li,Z., Foeth, E-J. *Cavitation Erosion-A review of Physical Mechanisms and Erosion Risk Models*, 7th International Symposium on Cavitation, CAV2009, Ann Arbor, Michigan, U.S.A.

[46] Jin Wang, 2009, *Nozzle-geometry-dependent breakup of diesel jets by ultrafast x-ray imaging: implication of in-nozzle cavitation*, Seventh Int. Symp. on Cavitation: CAV2009, Ann Arbor, Michigan, U.S.A.

[47] Watanabe, S., Furukawa, A., Yoshida, Y., Tsujimoto, Y., 2009, *Analytical investigations of thermodynamic effect on cavitation characteristics of sheet and tip leakage vortex cavitation*, Seventh Int. Symp. on Cavitation: CAV2009, Ann Arbor, Michigan, USA.

[48] Williams,M., Kawakami, E., Amromin, E., Arndt,R. *Effects of Surface Characteristics on Hydrofoil Cavitation*, Seventh Int. Symp. on Cavitation: CAV2009, Ann Arbor, Michigan, USA.

[49] Yoshimura,T., Kubota, S., Seo, T., Sato,K., 2009, *Development of Ballast Water Treatment Technology by Mechanochemical Cavitations*,Seventh Int. Symp. on Cavitation: CAV2009, Ann Arbor, Michigan, USA.

[50] Yount, D.E. 1979, *S*kins of Varying Permeability: A Stabilization Mechanism For Gas Cavitation Nuclei,A. ACCOUST. SOC. AM. 65(6).

Appendix A

Air Content of Water

The amount of air dissolved in water α can be expressed in many ways. The most common ways in literature are

- the gas fraction in weight ratio α_w
- the gas fraction in volume ratio α_v
- the molecule ratio
- the saturation rate
- the partial pressure of air

A.1 Solubility

Air is a mixture of 21 percent oxygen, 78 percent nitrogen and one percent of many other gases, which are often treated as nitrogen. The specific mass of gases involved in air are:

Oxygen (O_2)	1.429	kg/m^3
Nitrogen (N_2)	1.2506	kg/m^3
Air	1.292	kg/m^3

The maximum amount of gas that can be dissolved in water, the solubility), depends on pressure and temperature. It decreases with increasing temperature and increases with increasing pressure. The solubility of oxygen in water is higher than the solubility of nitrogen. Air dissolved in water contains approximately 36 percent oxygen compared to 21 percent in air.The remaining amount can be considered as Nitrogen. Nuclei which are in equilibrium with saturated water therefore contain 36 percent oxygen. But nuclei which are generated from the air above the water contain 21 percent oxygen. Since the ratio between oxygen and nitrogen is not fixed, it is difficult to relate measurements of dissolved oxygen (by osmose) to measurements of dissolved air (from e.g a van Slijke apparatus).

The amount of oxygen dissolved in water at atmospheric pressure at 15 degrees Celcius is approximately $10 * 10^-6 kg/kg$. For nitrogen this value is about $15 * 10^-6$, so the solubility of air in water is the sum of both: $25 * 10^-6$. Here the dissolved gas contents are expressed as a weigth ratio α_w.Air is very light relative to water and the weight ratio is very small. This ratio is therefore often expressed as parts per million (in weight), which is $10^6 * \alpha_w$.

A.2 The Gas Fraction in Volume Ratio

The volume of gas dissolved per cubic meter of water depends on temperature and pressure. Therefore this volume ratio is expressed in *standard conditions* of 0 degrees Celcius and 1013 mbar (atmospheric conditions). The dependency of the volume of water on temperature and pressure is neglected. The volume of the dissolved air is then described by the law of Boyle-Gay-Lussac:

$$\frac{p * Vol}{273 + T} = constant \tag{A.1}$$

The volume fraction at (p,T) can be related to the volume fraction in standard conditions:

$$\alpha_v = \alpha_v(p, T)\frac{273p}{(273 + T)1013} \tag{A.2}$$

The gas fraction in volume ratio is dimensionless (m^3/m^3). Be careful because sometimes this is violated by using cm^3/l ($1000 * \alpha_v$) or parts per million (ppm) which is $10^6 * \alpha_v$.

α_v is found from α_w by:

$$\alpha_v = \frac{\rho_{water}}{\rho_{air}}\alpha_w \tag{A.3}$$

in which ρ is the specific mass in kg/m^3. At 15 deg. Celcius and 1013 mbar pressure the specific mass of water $\rho_w = 1000kg/m^3$ and the specific mass of air is $1.223kg/m^3$, so for air $\alpha_v = 813\alpha_w$.

A.3 The Gas Fraction in Molecule ratio

The dissolved amount of gas can also be expressed as the ratio in moles(Mol/Mol). Molar masses may be calculated from the atomic weight in combination with the molar mass constant (1 g/mol) so that the molar mass of a gas or fluid in grams is the same as the atomic weight.
The molar ratio α_m is easily found from the weight ratio by

$$\alpha_w = \alpha_m\frac{M_(water)}{M_(gas)} \tag{A.4}$$

in which M is the molar weight, which is 18 for water, 16 for oxygen(O_2) and 28 for Nitrogen (N_2). For air a virtual molar weigth can be defined using the ratio of oxygen and nitrogen of 21/79 this virtual molar weight of air is about 29.

A.4 The saturation rate

The saturation rate is the amount of gas in solution as a fraction of the maximum amount that can go in solution in the same conditions. Since the saturation rate is dimensionless. It is independent of the way in which the dissolved gas or the solubility is expressed. The saturation rate is important because it determines if and in which direction diffusion will occur at a free surface. The saturation rate varies with temperature and pressure, mainly because the solubility of gas changes with these parameters.

A.5 The partial pressure

Sometimes the amount of dissolved gas is expressed as the partial pressure of the gas (mbar or even in mm HG). This is based on Henry's law, which states that the amount of gas dissolved in a fluid is proportional to the partial pressure of that gas. In a van Slijke apparatus a specific volume of water is taken and subjected to repeated spraying in near vacuum conditions (a low pressure decreases the solubility). This will result in collecting the dissolved in a chamber of specific size. By measuring the pressure in that chamber the amount of dissolved gas is found. Note that this pressure is not directly the partial pressure. A calibration factor is required which depends on the apparatus.

Appendix B

Standard Cavitators

A standard cavitator is a reference body which can be used to compare and calibrate cavitation observations and measurements. Its geometry has to be reproduced accurately and therefore an axisymmetric headform has been used as a standard cavitatior.

Such an axisymmetric body has been investigated in the context of the ITTC (International Towing Tank Conference).This is a worldwide conference consisting of towing tanks (and cavitation tunnels) which have the goal of predicting the hydrodynamic behavior of ships. To do that model tests and calculations are used. They meet every three years to discuss the state of the art and to define common problem areas which have to be reviewed by committees. The ITTC headform has a flat nose and an elliptical contour [22]. Its characteristics are given in Fig B.1.

This headform has been used to compare cavitation inception conditions and cavitation patterns in a range of test facilities. The results showed a wide range of inception conditions and also a diversity of cavitation patterns in virtually the same condition, as illustrated in Fig B.3. This comparison lead to the investigation of viscous effects on cavitation and cavitation inception.

The simplest conceivable body to investigate cavitation is the hemispherical headform. This is an axisymmetric body with a hemispere as the leading contour. Its minimum pressure coefficient is -0.74. The hemisperical

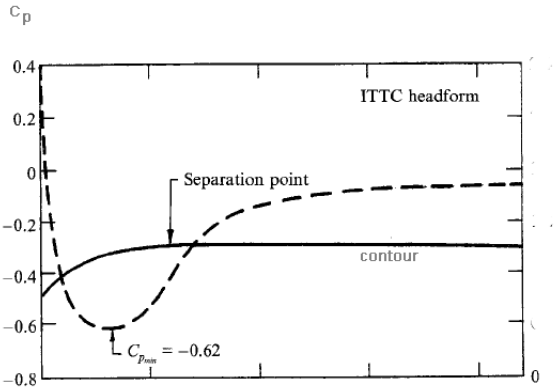

Figure B.1: Contour and Pressure Distribution on the ITTC Headform [31]

headform was used to compare inception measurements in various cavitation tunnels. However, it was realized later on that the boundary layer flow on both the ITTC and on the hemisperical headform was not as simple as the geometry suggested. In most cases the Reynolds numbers in the investigations was such that the boundary layer over the headform remained laminar and the pressure distribution was such that a laminar separation bubble occurred, in the position indicated in Fig. B.1. This caused viscous effects on cavitation inception and made the headform less suitable as a standard body. Note that the location of laminar separation is independent of the Reynolds number. When the Reynolds number becomes high transition to turbulence occurs upstream of the sep-

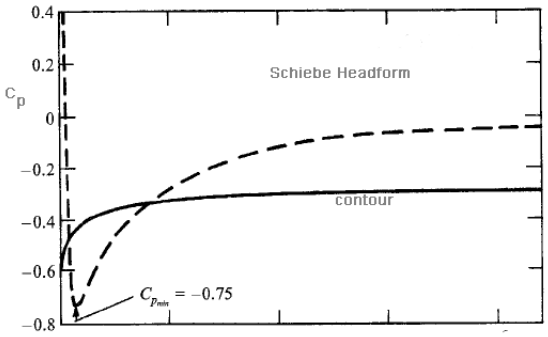

Figure B.2: Contour and Pressure Distribution of the Schiebe body [31]

aration location and separation will disappear.

To avoid laminar separation another headform was developed by Schiebe ([43]) and this headform bears his name ever since. The contour and pressure distribution on the Schiebe headform are given in Fig. B.2. This headform has no laminar separation and transition to a turbulent boundary layer will occur at a location which depends on the Reynolds number.

Many other headform shapes have been investigated with different minimum pressure coefficients and pressure recovery gradients.(e.g.[20])

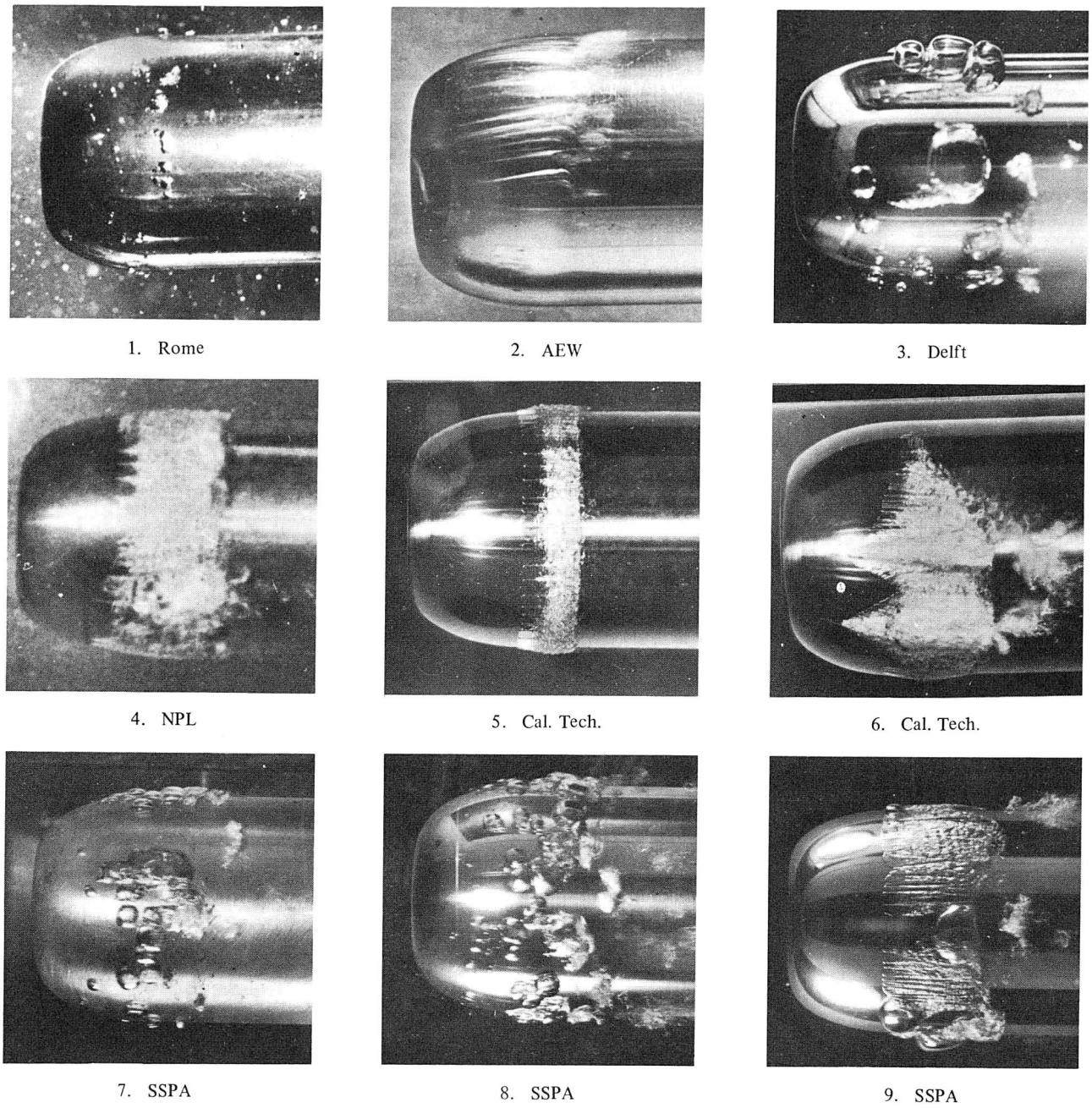

Figure B.3: Comparative measurements of cavitation inception on the ITTC headform source:ITTC

Appendix C

Tables

T Celcius	p_v N/m^2
0	608.012
2	706.078
4	813.951
6	932
8	1069
10	1226
12	1402
14	1598
15	1706
16	1814
18	2059
20	2334
22	2638
24	2981
26	3364
28	3785
30	4236
32	4756
34	5315
36	5943
38	6619
40	7375

Table C.1: Vapor pressure of Water.

Temp. deg. C.	kinem. visc. fresh water $m^2/sec \times 10^6$	kinem. visc. salt water $m^2/sec \times 10^6$
0	1.78667	1.82844
1	1.72701	1.76915
2	1.67040	1.71306
3	1.61665	1.65988
4	1.56557	1.60940
5	1.51698	1.56142
6	1.47070	1.51584
7	1.42667	1.47242
8	1.38471	1.43102
9	1.34463	1.39152
10	1.30641	1.35383
11	1.26988	1.31773
12	1.23495	1.28324
13	1.20159	1.25028
14	1.16964	1.21862
15	1.13902	1.18831
16	1.10966	1.15916
17	1.08155	1.13125
18	1.05456	1.10438
19	1.02865	1.07854
20	1.00374	1.05372
21	0.97984	1.02981
22	0.95682	1.00678
23	0.93471	0.98457
24	0.91340	0.96315
25	0.89292	0.94252
26	0.87313	0.92255
27	0.85409	0.90331
28	0.83572	0.88470
29	0.81798	0.86671
30	0.80091	0.84931

Table C.2: Kinematic viscosities adopted by the ITTC in 1963

R_n	$C_f \times 10^3$
1×10^5	8.333
2	6.882
3	6.203
4	5.780
5	5.482
6	5.254
7	5.073
8	4.923
9	4.797
1×10^6	4.688
2	4.054
3	3.741
4	3.541
5	3.397
6	3.285
7	3.195
8	3.120
9	3.056
1×10^7	3.000
2	2.669
4	2.390
6	2.246
8	2.162
1×10^8	2.083
2	1.889
4	1.721
6	1.632
8	1.574
1×10^9	1.531
2	1.407
4	1.298
6	1.240
8	1.201
1×10^{10}	1.17x

Table C.3: Friction coefficients according to the ITTC57extrapolator.

Temp. deg. C.	density fresh water kg/m^3	density salt water kg/m^3
0	999.8	1028.0
1	999.8	1027.9
2	999.9	1027.8
3	999.9	1027.8
4	999.9	1027.7
5	999.9	1027.6
6	999.9	1027.4
7	999.8	1027.3
8	999.8	1027.1
9	999.7	1027.0
10	999.6	1026.9
11	999.5	1026.7
12	999.4	1026.6
13	999.3	1026.3
14	999.1	1026.1
15	999.0	1025.9
16	998.9	1025.7
17	998.7	1025.4
18	998.5	1025.2
19	998.3	1025.0
20	998.1	1024.7
21	997.9	1024.4
22	997.7	1024.1
23	997.4	1023.8
24	997.2	1023.5
25	996.9	1023.2
26	996.7	1022.9
27	996.4	1022.6
28	996.2	1022.3
29	995.9	1022.0
30	995.6	1021.7

Table C.4: Densities as adopted by the ITTC in 1963.

Appendix D

Nomenclature

ρ	density of water	$\frac{kg}{m^3}$	See TableC.4
C_g	gas concentration	kg/m^3	see Appendix A
D_g	diffusion coefficient	m^2/sec	representative value $2 * 10_9$
D	diameter	m	
F_d	drag	N	
g	acceleration due to gravity	$\frac{m}{sec^2}$	Taken as 9.81
Nd	number density of nuclei	m^-4	
p_g	gas pressure	$fracNm^2$	
$fracNm^2$			
p_v	equilibrium vapor pressure		
R	radius	m	
μ	dynamic viscosity of water	$\frac{kg}{m*sec}$	
ν	kinematic viscosity of water	$\frac{m^2}{sec}$	$(\nu = \frac{\mu}{\rho})$See Table C.2
s	surface tension	Nm	for water 0.075